Research Article | Vol. 28, No. 22 / 26 October 2020 / Optics Express 32529
Optics EXPRESS

Direct patterning of periodic semiconductor nanostructures using single-pulse nanosecond laser interference

YUN-RAN WANG,[1] SANTIAGO M. OLAIZOLA,[2,3] IM SIK HAN,[1] CHAO-YUAN JIN,[1,4] AND MARK HOPKINSON[1,*]

[1]Department of Electronic and Electrical Engineering, University of Sheffield, Sheffield S3 7HQ, United Kingdom
[2]CEIT-IK4, Manuel Lardizabal 15, 20018 Donostia/San Sebastián, Spain
[3]Universidad de Navarra, Tecnun, Manuel Lardizabal 13, 20018 Donostia/San Sebastián, Spain
[4]College of Information Science and Electronic Engineering, Zhejiang University, Hangzhou 310007, China
*m.hopkinson@sheffield.ac.uk

Abstract: We demonstrate an effective method for fabricating large area periodic two-dimensional semiconductor nanostructures by means of single-pulse laser interference. Utilizing a pulsed nanosecond laser with a wavelength of 355 nm, precisely ordered square arrays of nanoholes with a periodicity of 300 nm were successfully obtained on UV photoresist and also directly via a resist-free process onto semiconductor wafers. We show improved uniformity using a beam-shaping system consisting of cylindrical lenses with which we can demonstrate highly regular arrays over hundreds of square micrometers. We propose that our novel observation of direct pattern transfer to GaAs is due to local congruent evaporation and subsequent droplet etching of the surface. The results show that single-pulse interference can provide a rapid and highly efficient route for the realization of wide-area periodic nanostructures on semiconductors and potentially on other engineering materials.

1. Introduction

Sub-micron periodic and quasi-periodic structures have shown enormous potential in the fields of nanophotonics [1,2], plasmonics [3,4], bioengineering [5], magnetic storage [6], nanofluidics [7], etc. In particular, ordered arrays of semiconductor nanostructures (nanoholes, nanopillars, nanoislands) are of great significance for the realization of optoelectronic devices with enhanced performance. For example, silicon nanohole arrays with sub-wavelength periodicity display strong optical antireflection and light trapping effects within solar cells over a broad wavelength and wide angular range [8,9], whilst periodic two-dimensional III-V semiconductor nanostructures are able to precisely confine light propagation in three dimensions [10]. Arrays of nanoholes/nanoislands can also serve as templates for site-controlled quantum dot and nanowire growth [11–14]. To fabricate these nanostructures, many advanced techniques have been developed including electron beam lithography [15], ion beam lithography [16], nanoimprint lithography [17] and interference lithography [18]. However, amongst all these possibilities, laser interference lithography (LIL) [19–21] has a considerable advantage in the simplicity of a mask-less single-step exposure process which could be highly cost-effective for the high throughput fabrication of periodic micro- and nanostructures over a large area (~mm^2 to cm^2). LIL utilizes the interference of multiple coherent laser beams to produce one-, two- or even three-dimensional periodic features. A wide variety of interference patterns can be obtained by manipulating the beam configuration,

#397709 https://doi.org/10.1364/OE.397709
Journal © 2020 Received 13 May 2020; revised 22 Jul 2020; accepted 3 Aug 2020; published 14 Oct 2020

Optics EXPRESS

e.g., the number of laser beams, the angle of incidence, azimuthal angle, polarization and the phase difference [18].

Multi-beam LIL is commonly applied by means of a timed CW laser exposure of a photosensitive layer and then the transfer of the pattern by chemical development and etching. However, the interference pattern may be disturbed by configurational movements due to thermal instability or even airflows. Pulsed laser interference negates many of these issues, but there has been remarkably little work on photoresist exposure using short pulses. Ellman et al. [20] reported the use of pulsed laser interference to produce holes on positive photoresist layers. However, the structures were in a relatively small area and have only sub-micron periodicity (850 nm) which is in the range of conventional optical lithography and arguably not a major advancement. Perhaps the closest to our approach is that of single-pulse multi-beam interference lithography applied to the formation of large area photonic crystals in thick SU-8 polymer films [22]. However, the dimensions in this case are still on the large size compared to state-of-the-art semiconductor device processing. To that extent, we are about to report feature sizes down to sub-100 nm levels and a pattern pitch of 300 nm using our approach. It would also be advantageous as part of any fabrication process to dispense with the intermediate photoresist step and perform direct laser interference patterning (DLIP) [23–25] onto materials surfaces. Many excellent works have demonstrated the direct fabrication of one-dimensional or two-dimensional micro- and sub-micron structures on metals [23], polymers [24] and ceramics [25] typically by femto- or pico-second lasers with high peak powers, but in some cases with nanosecond lasers. In terms of semiconductor research, it has been demonstrated that one can directly pattern silicon surfaces using such an approach [26–29]. All these experiments were performed in air and the resulting nanostructures such as gratings and nanohole arrays are generated mainly by materials deformation or ablation. With regard to the patterning of III-V semiconductors, such as GaAs, nanoholes have been created on a SiO_2/GaAs surface via DLIP [30]. However, this process requires an intermediate SiO_2 deposition step which appears to act to some extent as the pattern transfer medium. It does not leave a clean GaAs surface and even if removed by chemical etching may leave contamination or defects. Moreover, the generated nanoholes show a pattern heterogeneity only over a relatively small area and exhibit only sub-micron (>600 nm) periodicity. For the achievement of ultra-flat processed semiconductor surfaces and for the kind of dimensional control needed in the semiconductor industry there are limitations in the usefulness of previously published approaches. To advance the industrial application of LIL, the reproducible formation of large area patterns with nanoscale periodicity and without photoresist or other transfer medium would be a significant step.

The fabrication of large area 2D nanostructures with a periodicity down to a few hundred nanometers through single-pulse DLIP is still a challenging task. To the best of our knowledge, the fabrication of nanohole arrays on semiconductors with a periodicity as small as 300 nm by single-pulse nanosecond laser interference has not been presented to date. Therefore, it is of great commercial and scientific interest to produce semiconductor nanostructures with small lattice pitches using a single laser shot. Large incident angles are needed in order to obtain a small interference pitch and in this case the laser spot on the surface of the sample becomes highly elliptical due to the projection of the gaussian beam on the highly angled surface. This leads to the problem of beam alignment when using multiple beams and accordingly a heterogeneous energy distribution within interference pattern, thus hindering the realization of large-scale patterning.

In this paper, we describe the optical arrangement and implementation of a single-pulse four-beam nanosecond laser interference system. To compensate for beam projection effects, a beam-shaping approach using cylindrical lens pairs has been introduced. Nanohole arrays with a periodicity as small as 300 nm were obtained on the surface of both a commercial photoresist layer in air and directly on an epitaxial GaAs wafer in vacuum. We attribute the direct pattern formation on the GaAs wafer to surface decomposition followed by self-etching. This approach

Optics EXPRESS

shows the capability for direct, rapid and high-throughput patterning on semiconductor surfaces via single-pulse nanosecond laser interference, paving the way toward a single-step in-situ fabrication of semiconductor nanostructures.

2. Pulsed laser interference lithography on UV photoresist

We first developed a bench-top LIL experimental system in order to verify the single pulse approach and investigate the use of beam-shaping techniques. The experiments were performed using a four-beam interference configuration, as illustrated in Fig. 1(a). A flash-lamp pumped Nd:YAG laser (Innolas Spitlight) in spatial mode TEM00 (Gaussian intensity profile) operating at the third harmonic wavelength of λ=355 nm, with a pulse width of 7 ns, a repetition rate of 5 Hz and a beam diameter of 5 mm served as the laser source. The laser beam was split into four sub-beams with identical intensity and optical path by three 50:50 beam splitters (BS1-3). After that, the four sub-beams were reflected by four symmetrically placed UV mirrors with azimuthal angles of 0°, 90°, 180° and 270°, and then recombined on the center of targeted sample surface at an incident angle of θ=58° in order to obtain the desired pattern periodicity of about 300 nm. A half-wave plate and a Glan-laser polarizer were utilized in the path of each beam to control the laser energy and polarization directions of four beams. The polarization states of four beams are set to TM mode. To achieve a single pulse exposure, an external shutter was used to pick a pulse from the 5Hz laser repetition by a timed opening based on the laser Pockels cell trigger signal.

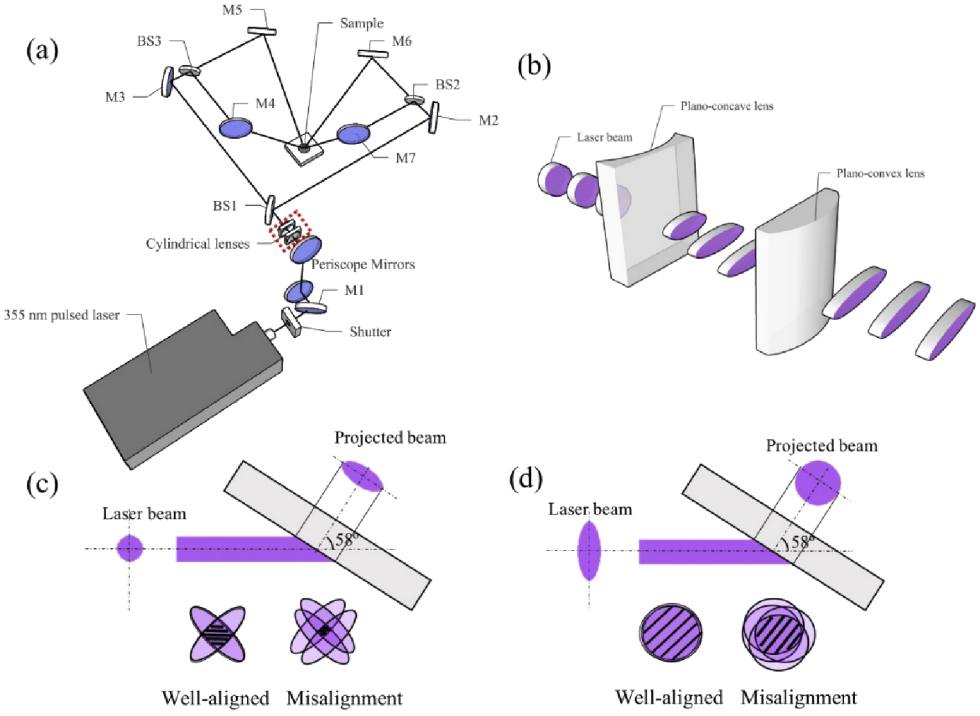

Fig. 1. (a) Schematic configuration of the four-beam laser interference optical setup with large an incident angle. BS1-BS3: 50:50 beam splitters; M1-M7: high reflective UV mirrors. (b) The enlarged diagram of the beam-shaping system as marked with a red dashed box shown in (a). Schematics of beam shape transformation due to the 58° incident angle and the corresponding alignment situations (c) without and (d) with the use of beam-shaping system.

In the optical path before BS1, a beam shaping system consisting of cylindrical lenses as presented in Fig. 1(b) was used to precondition the beam shape. A plano-concave cylindrical

Optics EXPRESS

lens of focal length f = −100 mm and a plano-convex cylindrical lens of focal length f = 200 mm was selected to obtain a magnification of 2. This uniaxial magnification along the horizontal axis pre-compensates the spot distortion generated by the non-perpendicular incident angle. Figure 1(c) shows a diagram describing the laser beam projection without the use of beam-shaping lenses and the corresponding overlapping area at the targeted surface. Even if the beams are well-aligned, they cannot completely overlap due to the elliptical beam shape. Also, several areas around the main interference spot are irradiated with non-desired two-beam interference. In comparison, with the help of the beam shaping system, the laser beam is converted into an elliptical shape at the input of the interference system, so that the elliptical pre-condition offsets the ellipticity caused by the beam projection and produces a round spot. The spot size on the sample surface after the beam shaping was approximately ~10 mm in diameter. A positive photoresist (PR) AZ 1514H (MicroChemicals) was used to record the interference patterns. PR films were spin coated onto clean 2-inch silicon wafers at a speed of 4000 rpm for 30 seconds with a thickness of approximately 1.7 μm, followed by a soft bake on a hot plate for 1 min at

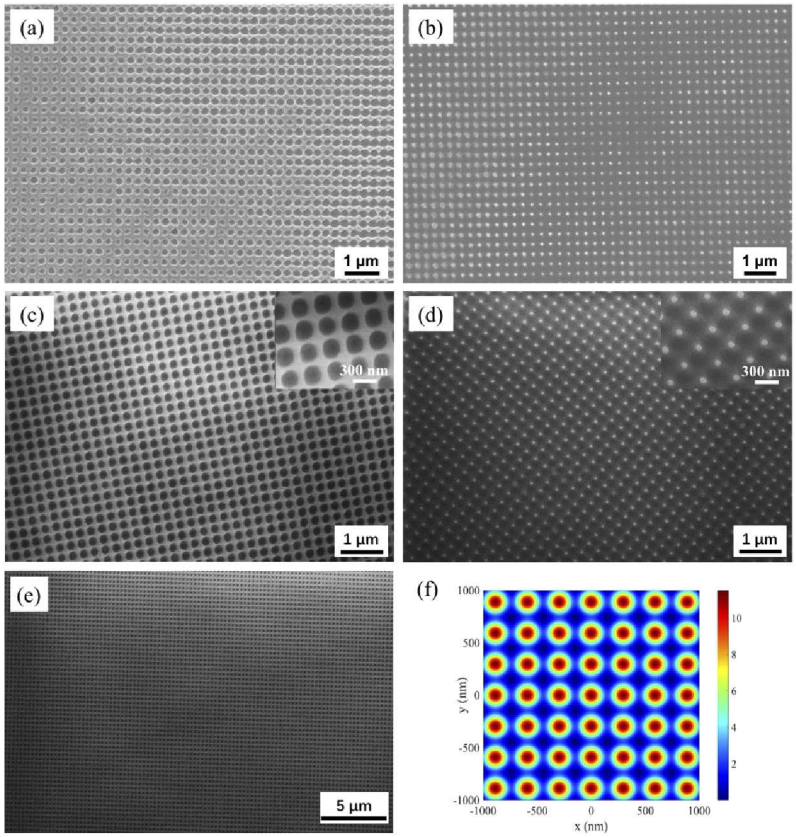

Fig. 2. SEM images of the fabricated 2D nanostructures on positive PR coated silicon wafers without beam-shaping of (a) nanoholes and (b) nanodots; with beam-shaping of (c) nanoholes and (d) dot-like structures. The pattern periodicity Λ=300 nm. Insets show the corresponding enlarged images. The laser fluences used were (a) 23 mJ/cm^2, (b) 33 mJ/cm^2, (c) 20 mJ/cm^2, and (d) 27 mJ/cm^2, respectively. (e) A 20×30 μm^2 SEM image of the nanohole array in (c). (f) MATLAB simulation result of the four-beam interference pattern with a lattice period of Λ=296 nm. The angle of incidence is 58° and the polarization state of all beams is set to the TM mode.

Optics EXPRESS

100°C. After that, the samples were exposed in air using single-pulse LIL with laser fluences of 20-35 mJ/cm^2 used to expose the resists. The samples were developed using an AZ developer for 10-15 seconds and finally were rinsed with deionized water and dried with nitrogen. The surface morphologies of the samples were characterized by scanning electron microscopy (SEM).

SEM images of two-dimensional square arrays of nanostructures, observed either as nanoholes or nanodots depending on the exposure and development conditions and fabricated without (a, b) and with (c, d) the use of beam-shaping optics is shown in Fig. 2. The fabricated structures here tend to be relatively shallow features as a result of the thick photoresist. With exposure at lower laser fluences of ~20 mJ/cm^2, the exposed regions (interference maxima) were dissolved into the developer leading to hole-like structures on the surface which can be seen in Fig. 2(a) and (c). At slightly higher laser fluences (~30 mJ/cm^2), as illustrated in Fig. 2(b) and (d), the pattern transforms to nanodot-like structures, where the dots are located at the interference minima regions. The obtained periodicity is around 300 nm in all samples and is consistent with the simulation results shown in Fig. 2(f), where the lattice period $\Lambda=\sqrt{2}\lambda/2\sin\theta$. In Fig. 2(a) and (b), we can see size variations over the imaging area, whilst the nanostructures in Fig. 2(c) and (d) have relatively uniform size and shape, with an average size of the holes of 200 nm in diameter and of the nanodot diameter of about 50 nm. Figure 3(e) shows that the uniformity of the nanohole array fabricated using beam shaping optics extends over hundreds of μm^2. In terms of even larger areas (eg: mm^2), the uniformity is affected by a Gaussian beam distribution which is a natural consequence of using relatively long beam paths. Large area uniformity is also compromised by Moiré effects [31] which originate from small variations in the individual beam paths. Further work is underway to improve these aspects with additional optics and alternative beam configurations. Nevertheless, these results provide important verification of the ability to perform single shot pulsed laser exposure to form nanoscale periodic features. We are not aware of any other techniques which could produce uniform arrays of such features over hundreds of μm^2 with a single short (7 ns) exposure process.

Optics EXPRESS

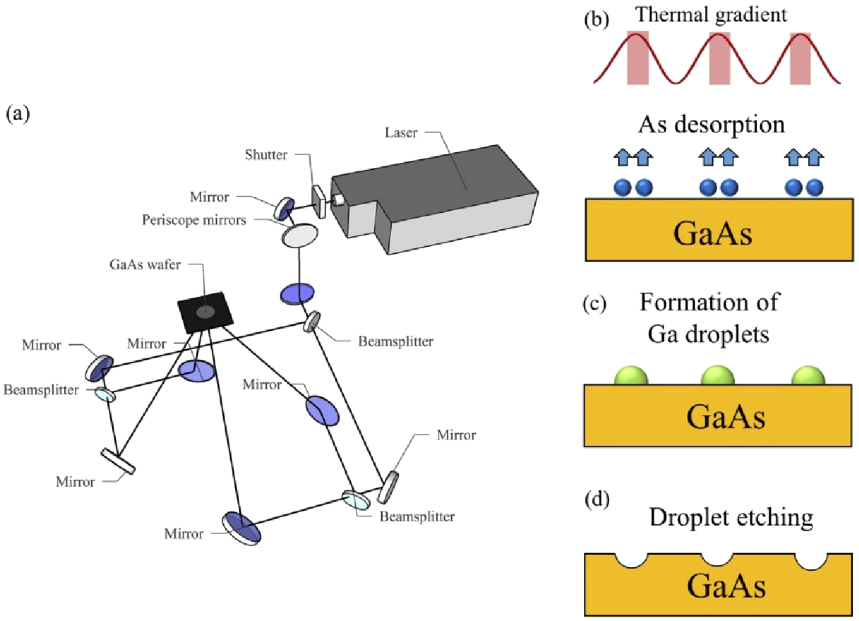

Fig. 3. (a) Schematics of a four-beam DLIP configuration with the MBE system. Schematic processes of Ga droplet etching steps. (b) As atom desorption due to interference-induced thermal gradient on the GaAs surface. (c) The formation of liquid Ga liquid droplets on the surface. (d) Local droplet etching results in the formation of nanohole arrays.

3. In-situ direct laser interference patterning (epitaxial GaAs wafers)

For the in-situ DLIP experiments on semiconductor substrates, another interference setup with a similar beam configuration was built. This system is based around a modified solid-source molecular beam epitaxy (MBE) growth system and has the optical configuration as shown in Fig. 3(a). The MBE system allows us to expose reactive surfaces in ultra-high vacuum and to provide stabilizing species to the semiconductor surface where necessary. It also will allow us to perform epitaxial growth on the exposed surfaces. However, for the work described herein, the MBE chamber is just used to prepare a clean and atomically flat GaAs surface for patterning experiments and to stabilize that surface against decomposition with a beam of excess arsenic. We used a flipper mirror to guide the output laser beam towards the MBE chamber. Four sub-beams were guided upwards through four symmetrically arranged antireflection fused silica optical viewports into the chamber and then converged on the center of the growing wafers, which allows the direct patterning to proceed simultaneously with the sample growth processes. Each optical beam path is identical, and the path lengths are ~3.5 m.

Two-inch epi-ready GaAs (100) wafers were prepared as follows. After surface native oxide desorption at (~620°C), a 1 μm-thick GaAs buffer layer was grown at a substrate temperature of 600°C for the purposes of smoothing the as-received surface, after which the temperature was cooled to 500°C when the growth of a final 500 nm of GaAs took place. Surfaces prepared in this way typically demonstrate monolayer (ML) flat surfaces with occasional meandering terraces. After this final GaAs growth, the substrates were immediately exposed by a single laser interference pulse (7 ns) inside the UHV MBE chamber with a stabilizing As flux maintained. Finally, the samples were subsequently quenched and taken out for characterization by atomic force microscopy (AFM) using tapping mode in air.

Optics EXPRESS

Different beam polarizations and laser fluences in the range of 20-45 mJ/cm^2 have been explored. The polarization of the laser beams determines the intensity profile of the interference pattern and also leads to a different spatial periodicity in four-beam interference. As displayed in the simulations, Figs. 4(a) and 4(b) show the interference patterns with the TM polarization state, while Fig. 4(c) presents the TE polarization. The difference between Figs. 4(a) and 4(b) is that in Fig. 4(a) all the beams are equal intensity and Fig. 4(b) shows the pattern with an unequal laser intensity which could exist on some areas of the pattern due to different beam overlap positions. A smaller lattice period Λ=209 nm is produced using the TE mode compared with a period of Λ=296 nm for the TM mode. However, the TM mode exhibits much better intensity contrast. Figures 4(d)–4(f) shows AFM images of four-beam interference patterns on GaAs surfaces using the TM mode with different laser fluences and intensity ratios. At the lowest fluence, in Fig. 4(d), we can just observe the formation of shallow holes at the interference maxima with materials accumulated around these holes. We assume the formation of this type of structure is due to surface mass transport. According to our previous photothermal model [32], local heat is produced on the GaAs substrate due to the strong surface absorption of UV laser energy. Consequently, the surface temperature at the interference maxima rises rapidly after the short 7 ns pulse exposure and the surface exhibits a two-dimensional periodic thermal gradient distribution. When their thermal energy exceeds the diffusion activation energy [32], atoms are able to move from the interference maxima towards the minima regions. With higher laser fluence, significantly deeper nanohole arrays (~3-4 nm) are formed at the interference maxima regions, as shown in Fig. 4(e). Although we can still see some material piled up on the edge of the holes, we cannot entirely attribute the formation of holes to the mass transport of material. We propose the following mechanism to explain the formation of these deeper nanoholes on the GaAs surface. When the surface temperature is sufficient high (>620°C) due to a high laser fluence, the decomposition of GaAs occurs due to the congruent evaporation of As, leaving behind free Ga atoms on the surface which will amalgamate to form Ga-rich liquid droplets [33]. Ga droplets are well known to self-etch the GaAs surface and to create nanoholes [34,35] and the shape of these 'droplet etched' surfaces is remarkably similar to our observations. When the laser fluence is insufficient to raise the surface temperature above the congruent temperature, the surface migration of materials is dominant. It can also be confirmed from Fig. 4(f) which corresponds to the situation represented by the simulation in Fig. 4(b). These shallow patterns, resulting monolayer variations in the surface height have a close relationship to the calculated intensity profiles because they are simply formed by the mass transport of materials.

In terms of TE polarization, 1D gratings, 2D shallow hole arrays and checkerboard gratings with a period of $\Lambda\approx$210 nm can be fabricated as shown in Figs. 4(g)–4(i). There is no obvious formation of holes, which could be attributed to the relatively lower laser energy absorbed on the GaAs owing to the much higher surface reflectance for the TE mode [36]. It could also be associated with the poorer intensity contrast in this case. For these reasons, shallow or 'weak' pattern features resulting from surface atom migration is characteristics of structures produced using the TE mode.

Therefore, by adopting appropriate beam polarization and laser fluence, precisely ordered arrays of nanoholes with a period of 300 nm can be fabricated on the GaAs surface with a single laser pulse. As shown in Fig. 5(a), an almost clean surface with uniform nanoholes were obtained. The corresponding 3D AFM image and cross-sectional profiles of the nanoholes are shown in Figs. 5(c) and 5(e) respectively. The nanoholes typically have a shallow depth of ~3 nm and an average width of ~120 nm. At a higher laser fluence of 46 mJ/cm^2, as seen in the Fig. 5(b) we observed the formation of the same nanoholes, but also can see the formation of many small islands or droplet-like features in between the holes. The magnified 3D image and the line profile across the nanoholes for this higher fluence is shown in Figs. 5(d) and 5(f). The depth and width of the holes are approximately the same as those in the case of Fig.

Optics EXPRESS

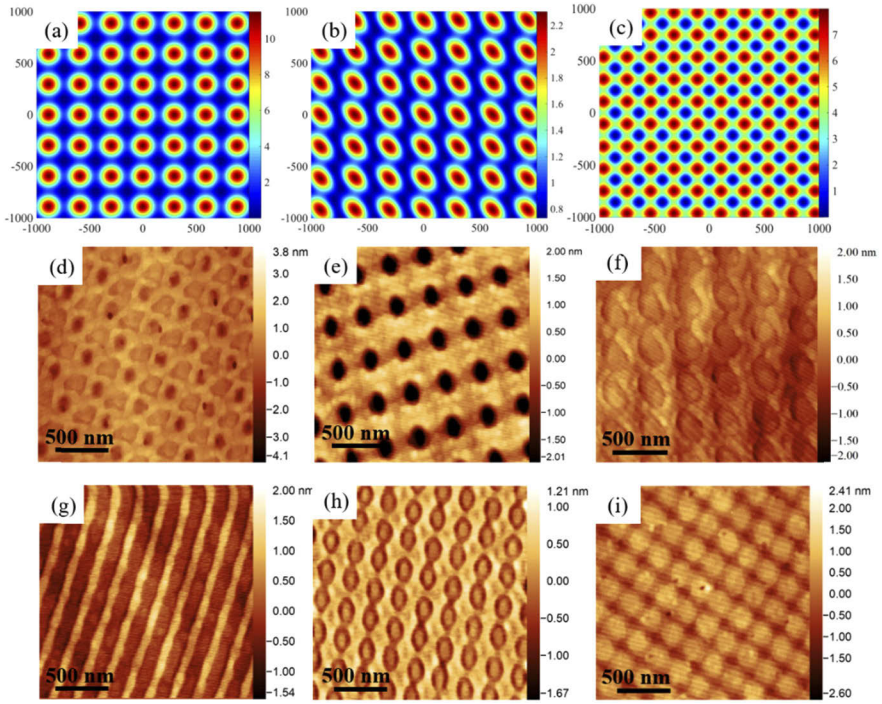

Fig. 4. Simulations of four-beam interference pattern with an incident angle of 58° using different polarization states (a, b) TM mode and (c) TE mode; (b) unequal laser intensity ratio of four beams 0.4:0.1:1:0.4. AFM images of four-beam interference pattern (Λ≈300 nm) in TM mode with different laser fluences of (d) 22 mJ/cm^2, (e, f) 38 mJ/cm^2, and (f) corresponds to the simulation in (b). (g) Grating formed by two-beam interference in TE mode, with a fluence of 28 mJ/cm^2. (h, i) Four-beam interference in TE mode (Λ≈210 nm), with different fluences of 31 mJ/cm^2 and 45 mJ/cm^2, respectively.

5(a). Our experiments were carried out in an epitaxy environment in which the substrate base temperature is already at 500°C. With the additional temperature increase due to photothermal absorption of the laser pulse, the surface temperature can easily reach several tens or hundreds of degrees above this base temperature. In the case of Fig. 5(a), at the interference maxima regions we believe, the temperature has exceeded the congruent evaporation temperature of GaAs, estimated to be around 680°C [34]. However, this is only reached at the narrow maxima regions and in other regions the temperature does not reach this threshold. A relatively small region containing liquid Ga is formed and this etches small nanoholes. At higher laser fluence much larger thermal gradients are created on the surface and under those conditions Ga atoms formed through congruent evaporation may be able to diffuse from the high-temperature area to the low-temperature area. This free Ga forms small droplets all over the surface and will recrystallize as GaAs as the temperature is reduced. These small GaAs droplets are all over the flat regions of the surface in Fig. 5(b).

This technique takes the advantage of material growth and laser interference patterning to fabricate periodic arrays of semiconductor nanostructures with a small lattice pitch using relatively low pulse energies when compared to ablation or deformation processes. In this case, we believe that the GaAs remarkably acts as its own ‘photoresist’ and ‘etchant’. For the heterogeneous fabrication of nanostructures, it is very beneficial to maintain the atomic smoothness and absolute cleanliness of the sample surface by combining lateral patterning and epitaxial growth in the

Optics EXPRESS

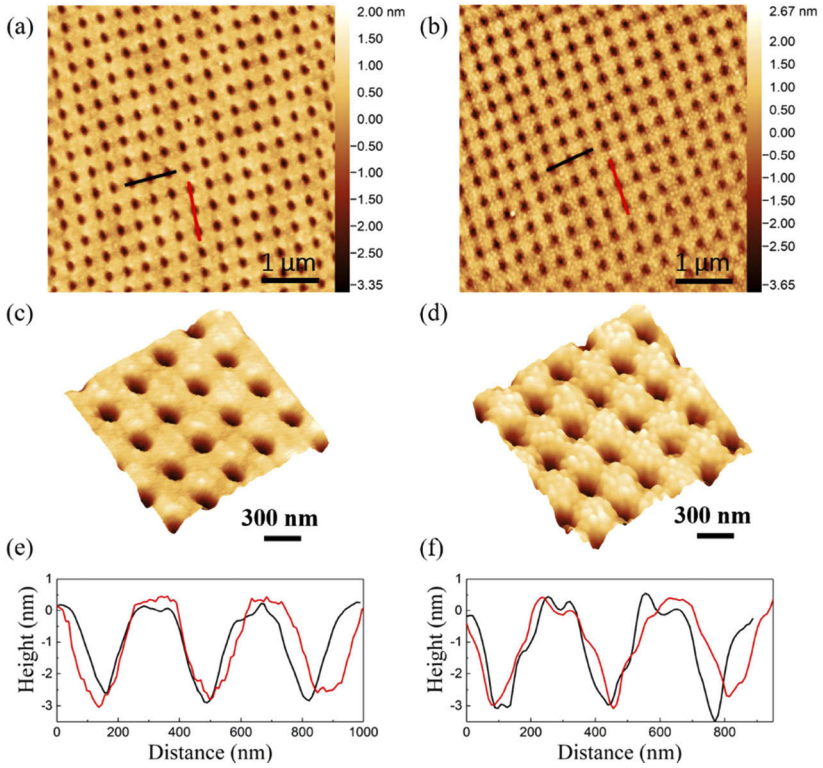

Fig. 5. AFM images of the fabricated nanohole arrays with a period of $\Lambda \approx 300$ nm on GaAs (100) substrates after the single-pulse four-beam interference patterning with different laser fluences of (a) 35 mJ/cm^2 and (b) 46 mJ/cm^2, respectively. (c-d) The corresponding 3D AFM images. (e-f) The corresponding line profiles of nanoholes along the directions marked with black and red lines in (a-b).

same vacuum environment. In addition, single pulse patterning is very favorable for growth systems such as MBE for which it is difficult to achieve low vibration due to the use of mechanical vacuum pumps and wafer mounting systems which do not tightly retain the wafer to allow for thermal expansion. With a 7 ns exposure time these vibration issues become negligible. Finally, we should state that although these observations are specific to GaAs there is no reason to believe they could not be applied to other semiconductors or indeed to other materials based on other thermodynamic or surface chemical changes under interference patterning.

4. Conclusions

We have presented the fabrication of two-dimensional periodic nanostructures with a periodicity of 300 nm on semiconductor surfaces using both conventional photoresist and also directly onto GaAs substrates by using a single-pulse exposure from an optical setup of four-beam nanosecond laser interference in combination with a beam-shaping system. The pre-conditioning of the beam shape prior to the interference compensates for the ellipticity caused by the beam projection and therefore creates an improved beam spot, contributing to realizing a more uniform multi-beam interference area. We propose that our observations of the direct patterning of GaAs are due to a process of local congruent evaporation and self-etching. This technique shows enormous potential for rapid, large-scale and high-efficient fabrication of two-dimensional nanohole arrays on III-V and perhaps on other semiconductor surfaces for potential applications such as in

Optics EXPRESS

photonic crystals, antireflective coatings and in the production of templates for semiconductor quantum dot or nanowire epitaxy.

Funding

H2020 Excellent Science (767285 'Nanostencil'); and Engineering and Physical Sciences Research Council (EP/P027822/1/).

Disclosures

The authors declare no conflicts of interest.

References

1. G. Von Freymann, A. Ledermann, M. Thiel, I. Staude, S. Essig, K. Busch, and M. Wegener, "Three-dimensional nanostructures for photonics," Adv. Funct. Mater. **20**(7), 1038–1052 (2010).
2. F. Priolo, T. Gregorkiewicz, M. Galli, and T. F. Krauss, "Silicon nanostructures for photonics and photovoltaics," Nat. Nanotechnol. **9**(1), 19–32 (2014).
3. M. E. Stewart, C. R. Anderton, L. B. Thompson, J. Maria, S. K. Gray, J. A. Rogers, and R. G. Nuzzo, "Nanostructured plasmonic sensors," Chem. Rev. **108**(2), 494–521 (2008).
4. N. C. Lindquist, P. Nagpal, K. M. McPeak, D. J. Norris, and S. H. Oh, "Engineering metallic nanostructures for plasmonics and nanophotonics," Rep. Prog. Phys. **75**(3), 036501 (2012).
5. Q. Luo, C. Hou, Y. Bai, R. Wang, and J. Liu, "Protein assembly: versatile approaches to construct highly ordered nanostructures," Chem. Rev. **116**(22), 13571–13632 (2016).
6. M. Albrecht, G. Hu, I. L. Guhr, T. C. Ulbrich, J. Boneberg, P. Leiderer, and G. Schatz, "Magnetic multilayers on nanospheres," Nat. Mater. **4**(3), 203–206 (2005).
7. S. Jeon, V. Malyarchuk, J. O. White, and J. A. Rogers, "Optically fabricated three-dimensional nanofluidic mixers for microfluidic devices," Nano Lett. **5**(7), 1351–1356 (2005).
8. J. Tippens, A. Bagal, X. A. Zhang, and C. H. Chang, "Nanostructured antireflective in-plane solar harvester," Opt. Express **25**(16), A840–A850 (2017).
9. S. E. Han and G. Chen, "Optical absorption enhancement in silicon nanohole arrays for solar photovoltaics," Nano Lett. **10**(3), 1012–1015 (2010).
10. E. Chow, S. Y. Lin, S. G. Johnson, P. R. Villeneuve, J. D. Joannopoulos, J. R. Wendt, and A. Alleman, "Three-dimensional control of light in a two-dimensional photonic crystal slab," Nature **407**(6807), 983–986 (2000).
11. J. Martín-Sánchez, G. Muñoz-Matutano, J. Herranz, J. Canet-Ferrer, B. Alén, Y. González, and F. Briones, "Single photon emission from site-controlled InAs quantum dots grown on GaAs (001) patterned substrates," ACS Nano **3**(6), 1513–1517 (2009).
12. Y. R. Wang, I. S. Han, C. Y. Jin, and M. Hopkinson, "Precise Arrays of Epitaxial Quantum Dots Nucleated by In-Situ Laser Interference for Quantum Information Technology Applications," ACS Appl. Nano Mater. **3**(5), 4739–4746 (2020).
13. Y. R. Wang, I. S. Han, C. Y. Jin, and M. Hopkinson, "Formation of laterally ordered quantum dot molecules by in situ nanosecond laser interference," Appl. Phys. Lett. **116**(20), 201901 (2020).
14. M. Hocevar, G. Mmink, M. Verheijen, N. Akopian, V. Zwiller, L. Kouwenhoven, and E. Bakkers, "Growth and optical properties of axial hybrid III–V/silicon nanowires," Nat. Commun. **3**(1), 1266 (2012).
15. C. Vieu, F. Carcenac, A. Pepin, Y. Chen, M. Mejias, A. Lebib, and H. Launois, "Electron beam lithography: resolution limits and applications," Appl. Surf. Sci. **164**(1-4), 111–117 (2000).
16. F. Watt, A. A. Bettiol, J. A. Van Kan, E. J. Teo, and M. B. H. Breese, "Ion beam lithography and nanofabrication: a review," Int. J. Nanosci. **04**(03), 269–286 (2005).
17. L. J. Guo, "Nanoimprint lithography: methods and material requirements," Adv. Mater. **19**(4), 495–513 (2007).
18. C. Lu and R. H. Lipson, "Interference lithography: a powerful tool for fabricating periodic structures," Laser Photonics Rev. **4**(4), 568–580 (2010).
19. A. Rodriguez, M. Echeverría, M. Ellman, N. Perez, Y. K. Verevkin, C. S. Peng, and S. M. Olaizola, "Laser interference lithography for nanoscale structuring of materials: From laboratory to industry," Microelectron. Eng. **86**(4-6), 937–940 (2009).
20. M. Ellman, A. Rodríguez, N. Pérez, M. Echeverria, Y. K. Verevkin, C. S. Peng, and I. Ayerdi, "High-power laser interference lithography process on photoresist: Effect of laser fluence and polarisation," Appl. Surf. Sci. **255**(10), 5537–5541 (2009).
21. M. Vala and J. Homola, "Flexible method based on four-beam interference lithography for fabrication of large areas of perfectly periodic plasmonic arrays," Opt. Express **22**(15), 18778–18789 (2014).
22. M. Campbell, D. Sharp, M. Harrison, R. Denning, and A. Turberfield, "Fabrication of photonic crystals for the visible spectrum by holographic lithography," Nature **404**(6773), 53–56 (2000).
23. M. Bieda, M. Siebold, and A. F. Lasagni, "Fabrication of sub-micron surface structures on copper, stainless steel and titanium using picosecond laser interference patterning," Appl. Surf. Sci. **387**, 175–182 (2016).

Optics EXPRESS

24. S. Alamri and A. F. Lasagni, "Development of a general model for direct laser interference patterning of polymers," Opt. Express **25**(9), 9603–9616 (2017).
25. J. Berger, M. G. Holthaus, N. Pistillo, T. Roch, K. Rezwan, and A. F. Lasagni, "Ultraviolet laser interference patterning of hydroxyapatite surfaces," Appl. Surf. Sci. **257**(7), 3081–3087 (2011).
26. D. Wang, Z. Wang, Z. Zhang, Y. Yue, D. Li, and C. Maple, "Direct modification of silicon surfaces by nanosecond laser interference lithography," Appl. Surf. Sci. **282**, 67–72 (2013).
27. C. Y. Zhang, J. W. Yao, H. Y. Liu, Q. F. Dai, L. J. Wu, S. Lan, and T. M. Lysak, "Colorizing silicon surface with regular nanohole arrays induced by femtosecond laser pulses," Opt. Lett. **37**(6), 1106–1108 (2012).
28. V. Oliveira, R. Vilar, R. Serra, J. C. Oliveira, N. I. Polushkin, and O. Conde, "Sub-micron structuring of silicon using femtosecond laser interferometry," Opt. Laser Technol. **54**, 428–431 (2013).
29. M. Gedvilas, S. Indrišiūnas, B. Voisiat, E. Stankevičius, A. Selskis, and G. Račiukaitis, "Nanoscale thermal diffusion during the laser interference ablation using femto-, pico-, and nanosecond pulses in silicon," Phys. Chem. Chem. Phys. **20**(17), 12166–12174 (2018).
30. C. Tan, C. S. Peng, J. Pakarinen, M. Pessa, V. N. Petryakov, Y. K. Verevkin, and S. Tisserand, "Ordered nanostructures written directly by laser interference," Nanotechnology **20**(12), 125303 (2009).
31. Z. Zhang, L. Dong, Y. Ding, L. Li, Z. Weng, and Z. Wang, "Micro and nano dual-scale structures fabricated by amplitude modulation in multi-beam laser interference lithography," Opt. Express **25**(23), 29135–29142 (2017).
32. Y. R. Wang, C. Y. Jin, C. H. Ho, S. Chen, H. Francis, and M. Hopkinson, "Thermodynamic processes on a semiconductor surface during in-situ multi-beam laser interference patterning," IET Optoelectron. **13**(1), 7–11 (2019).
33. C. T. Foxon, J. A. Harvey, and B. A. Joyce, "The evaporation of GaAs under equilibrium and non-equilibrium conditions using a modulated beam technique," J. Phys. Chem. Solids **34**(10), 1693–1701 (1973).
34. C. Heyn and D. E. Jesson, "Congruent evaporation temperature of molecular beam epitaxy grown GaAs (001) determined by local droplet etching," Appl. Phys. Lett. **107**(16), 161601 (2015).
35. C. Heyn, S. Schnüll, D. E. Jesson, and W. Hansen, "Thermally controlled widening of droplet etched nanoholes," Nanoscale Res. Lett. **9**(1), 285 (2014).
36. Filmetrics Spectral Reflectance Calculator for Thin-Film Stacks. Available at https://www.filmetrics.com/reflectance-calculator. "Uses data for GaAs from J. B. Theeten, Aspnes, D. E.; R. P. H. Chang," J. Appl. Phys. **49**, 6097 (1978).